







# Foot-Controlled Robot-Enabled EnDOscope Manipulator (FREEDOM) for Sinus Surgery: Design, Control, and Evaluation

Fangxun Zhong , *Student Member, IEEE*, Peng Li , Jiadong Shi, *Member, IEEE*, Zerui Wang , *Member, IEEE*, Jiahao Wu , *Student Member, IEEE*, Jason Y. K. Chan , Natalie Leung, Iris Leung, Michael C. F. Tong, and Yun-Hui Liu , *Fellow, IEEE*

**Abstract**—Despite successful clinical applications, teleoperated robotic surgical systems face particular limitations in the functional endoscopic sinus surgery (FESS) in terms of incompatible instrument dimensions and robot set-up. The endoscope remains manually handled by an assistant when the surgeon performs bimanual operations. This paper introduces the development of the Foot-controlled Robot-Enabled EnDOscope Manipulator (FREEDOM) designed for FESS. The system features clinical considerations that inform the design for providing reliable and safe endoscope positioning with minimal obstruction to the routine practice. The robot structure is modular and compact to ensure coaxial instrument manipulation through the nostril for manual procedures. To avoid rigid endoscope motions, a new compliant endoscope holder is proposed that passively limits the lens-tissue contact forces under collisions for patient-side protection. To facilitate hands-free endoscope manipulation that imposes minimal distractions to the surgeon, a foot-wearable interface is further designed to relieve the assistant's workload. The foot control method owns a short learning curve (mean 3.4 mins), and leads the task to be more ergonomic and surgeon-centered. Cadaver and clinical studies were both conducted to evaluate the surgical applicability of the FREEDOM to assist endoscope manipulation in FESS. The

system was validated to be safe (IEC-60601-1) and easy for set up (mean 3.6 mins), from which the surgeon could perform various three-handed procedures alone in FESS without disrupting the routine practice.

**Index Terms**—Functional endoscopic sinus surgery (FESS), endoscope manipulation, passive compliance, control interface, robot-assisted surgery.

## I. INTRODUCTION

FUNCTIONAL endoscopic sinus surgery (FESS) is one of the most frequently performed surgeries in otorhinolaryngology [1]. By utilizing endoscopic inspections, the surgeon treats the diseased sinus area in a minimally-invasive manner by restricting the surgical procedures within the patient's nasal cavity [2]. This results in single-port access (SPA) with cluttered workspace which challenges the skills of the surgeon to manipulate instruments. In current practice, the surgeon continuously handles the endoscope with one hand, leaving the other for the surgical tool [3], [4]. An assistant is additionally required to hold the endoscope when the surgeon performs three-handed procedures (or THPs, requiring simultaneous manipulation of two instruments and an endoscope), e.g., suctioning, cauterization, tissue resection, etc. This could be unergonomic and could raise extra demand for surgeon-assistant collaboration skills [5]. As the trend of endoscopic surgeries is towards the integration of robotic technology [6], endowing robot-assisted endoscope manipulation (RAEM) to FESS could offer an advancement for surgeons with improved handling precision and reduced human workload [2], [3], [7].

Developing robotic systems for surgery proposes has been comprehensively reported [8]–[10]. The current paradigm of robot-assisted surgery in clinical practice is teleoperation led by the da Vinci Surgical System (dVSS) [9], which emphasizes the remote control of robotized instruments that keeps the primary surgeon from the operating table. Despite successful implementation to laparoscopic and transoral surgeries [1], [11], the system faces particular limitations in FESS that the instrument dimensions and robot set-up do not cater for the procedures [12], [13], or otherwise in a more invasive manner [4]. Dealing with the indirect manipulation requires substantial pre-clinical training by novice surgeons [14]. To share the surgical workload inside the operating theater (OT), improving adaption to

Manuscript received March 4, 2019; revised June 30, 2019 and August 6, 2019; accepted August 23, 2019. Date of publication September 5, 2019; date of current version May 20, 2020. This work was supported in part by the HK RGC under Grants T42-409/18-R and 14202918, in part by the Shenzhen Fundamental Research under Grant JCYJ20170307150346964, in part by the CUHK-SJTU Joint Research Fund under Project 4750352, and in part by the CUHK T Stone Robotics Institute, CUHK under VC Fund 4930745. (Corresponding author: Zerui Wang; Peng Li.)

F. Zhong, J. Wu, and Y-H. Liu are with the T Stone Robotics Institute, Department of Mechanical and Automation Engineering, The Chinese University of Hong Kong.

Z. Wang is with the T Stone Robotics Institute, Department of Mechanical and Automation Engineering, The Chinese University of Hong Kong, Hong Kong (e-mail: zrwang@mae.cuhk.edu.hk).

P. Li is with the School of Mechanical Engineering and Automation, Harbin Institute of Technology (Shenzhen), Shenzhen, Guangdong, China (e-mail: peng.li@hit.edu.cn).

J. Shi is with the School of Mechatronical Engineering, Beijing Institute of Technology.

J. Y. K. Chan, N. Leung, I. Leung, and M. C. F. Tong are with the Department of Otorhinolaryngology, Head and Neck Surgery, The Chinese University of Hong Kong.

This article has supplementary downloadable material available at <http://ieeexplore.ieee.org>, provided by the authors.

Digital Object Identifier 10.1109/TBME.2019.2939557

existing FESS routine practice with better operation safety and user friendliness becomes of great urgency to be solved by new robotic systems, which is also the primary motivation in this paper.

Existing research works have revealed applications of RAEM in sinus surgery. One typical approach is the utilization of commercialized industrial robot arms [15]–[20]. The major concern is that their structure and workspace design are not optimized for surgery purposes and could raise safety issues. RAEM was also explored by using surgical robots such as AESOP and SOLOASSIST [21]–[24]. However, the robots do not provide a mechanically-constrained remote center-of-motion (RCM), which is an important kinematic constraint for safe RAEM via single port access (SPA) in minimally-invasive surgeries [9]. To customize the robot design to FESS, Burgner *et al.* [25] developed a robotic system for endonasal skull base surgery. However, clinical evaluations in terms of system set-up and tool sterilizability inside the OT were not presented. Trévillot *et al.* [26] approached RAEM using a passive serial structure mounted on an industrial arm to clear the surgical space. Manual handling of the holder during FESS is still required by the surgeon. Sun *et al.* [27] introduced a light-weight endoscope holder using passive joints fixed on the operating table without RCM constraints. However, the above robot prototypes have not met the safety issue of robot-handled endoscope motions, which are normally rigid and own risks to harm the patient's nasal cavity once being misoperated. Furthermore, it is noteworthy that most of the aforementioned systems have not been evaluated at clinical stage.

As automated RAEM is yet not clinically available, dependency on the surgeon-in-the-loop surgery imposes demand for user control strategy such that the surgeon could master RAEM directly at his/her discretion. During the FESS, continual position adjustment of the endoscope is necessary as the narrow nasal cavity hinders a clear view of the surgical area. The control intuitiveness of the human-robot interface may exert great influence on the task effectiveness. In this regard, attempts have been made using master-slave teleoperation for surgeon-centered FESS procedures [12], [16], [25]. However, its capability to perform THPs using robot arms within the narrow passage is unclear. Kristin *et al.* [24] proposed a hand-controlled joystick installed at the rear end of an instrument. Aiming for hands-free control, voice recognition was adopted by the AESOP robot via clinical evaluations [21], [22], [28], whose shortcomings were exposed by voice disturbances from staff communication and misoperations led by poor recognition. In [29] and [30], the researchers further implemented eye-gaze control to surgical manipulators. Paddle control has been widely used by commercialized electrical medical devices and by a few surgical robotic systems [5], [10]. However, the implementation to RAEM may interfere the surgeon to use other paddle-operated devices (e.g., the cautery) during FESS, as multi-paddle control usually requires visual confirmation. There are also approaches that suggest preoperative CT scanning combined with automatic navigation and/or manipulation of endoscope during the surgery [18], [31], [32]. Automatic manipulation of the endoscope upon image-guided controllers has also been explored in [33], [34].

In this paper, we present a new robotic system FREEDOM (Foot-controlled Robot-Enabled EndoScope Manipulator) that aims for side-by-side RAEM with the surgeon in FESS. The contributions of this work include 1) a summary of clinical considerations for operational safety and user ergonomics, 2) a newly designed prototype featuring surgeon-centered configuration and minimal obstruction to routine practice, and 3) cadaver and clinical investigation of the system viability, which are weakly explored by existing approaches. The FREEDOM considerably complements our previous works in [35]–[37] by a newly designed passive-active combined joint set to accommodate for dexterous and RCM-constrained RAEM with staff-available space (see Fig. 1) for manual procedures. To improve patient-side safety, a novel passively-compliant endoscope holder (PCEH) is proposed (not met in [35], [37]) to avoid excessive interaction forces towards the nasal tissues in case of lens-tissue collision. The PCEH is pluggable, sterilizable, and compatible to the use of a lens sheath for lens tip cleaning. Based on [37], a foot-controlled user interface is developed with improved robust signal processing algorithm and a new voice indication system for hands-free pose adjustment of the endoscope, which has not appeared in existing surgical robots. The system performance is investigated via laboratory test and cadaver study, with its surgical viability inside the OT being further evaluated by clinical trials.

## II. DESIGN REQUIREMENTS

The main goal of the FREEDOM as a “surgical assistant” is to independently assist RAEM for FESS to enable THPs to be performed by the surgeon alone, instead of the regular two-surgeon approach, to improve task ergonomics. Meanwhile, a coupled requirement is to adapt to the routine practice of FESS. The robot should be easy to set up and should not obstruct the standing position and instrument manipulation space of the surgeon, as the SPA in FESS leads to a concentrated but crowded working environment around the patient's head. To facilitate coaxial instrument manipulation inside the nasal cavity in FESS, a constrained but reliable workspace should be provided for endoscope manipulation (an example endoscope workspace for sinus surgery is measured by Trévillot [26]).

Surgeon-side user friendliness and patient-side safety are also crucial factors that affect the surgical applicability of the system. As a result of hands-free endoscope manipulation, a control interface should be provided to the surgeon with intuitive user experience. The method should be easy to learn and should not impose major distractions to his/her bimanual procedures. As rigid robot-handled endoscope motions may increase risks for tissue damage to the patient under lens-tissue collisions, additional safety mechanism should also be designed for protection in case of misoperations.<sup>1</sup> During the surgery, cleaning the lens tip is common and should be done by using a lens sheath. The holder should be able to meet such issue and to allow independent sterilization.

To summarize, the design requirements of a robotic system to provide endoscope manipulation in clinical use should:

<sup>1</sup>The misoperation is defined as the robot motions being triggered unexpectedly without commands, or reacting incorrectly subject to interface control.

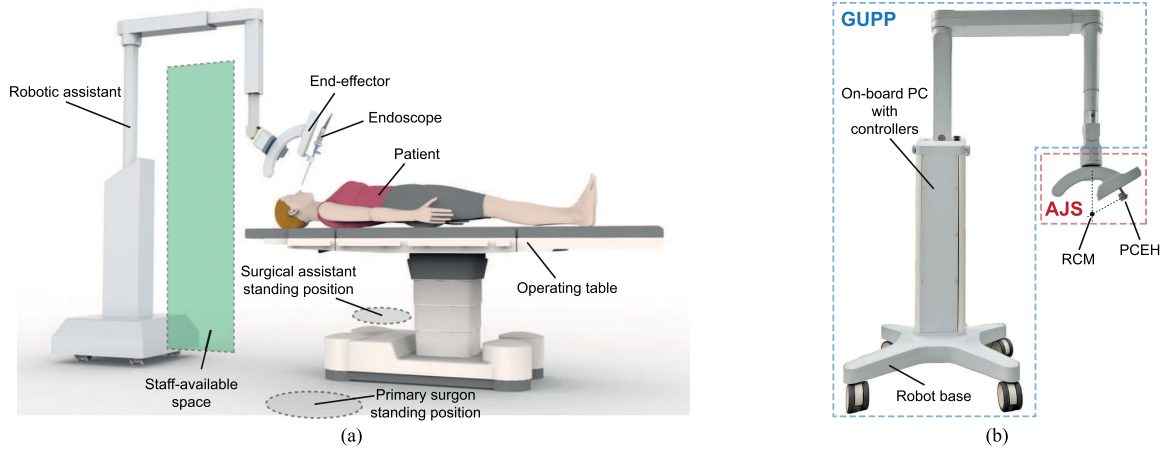


Fig. 1. (a) The expected set-up position for robot-assisted FESS that preserves ample working space for the surgical staff. Careful positioning of the FREEDOM is required to avoid impinging the surgeon. (b) The modular design of the FREEDOM with a robot base, a general-use passive platform (GUPP), an active joint set (AJS) and a passively-compliant endoscope holder (PCEH).

- 1) have a compact and dexterous structure for easy set-up which does not impose obstruction to the surgeon's routine practice;
- 2) provide the endoscope with a constrained workspace for RAEM under SPA for intraoperative adjustment;
- 3) provide an intuitive control method (better to be hands-free) for the surgeon to master RAEM alone intuitively;
- 4) provide patient-side protection in case of possible damage from misoperations;
- 5) meet the use of endoscopic lens sheath to ease the steps for lens cleaning process (as needed);
- 6) be compatible with other electrical devices in the OT.

### III. MECHANICAL DESIGN

#### A. General-Use Passive Platform (GUPP)

Fig. 2(a) shows the structural design of the GUPP. The mechanical structure of the GUPP should be able to determine the RCM position as well as giving an initial 3-DoF orientation of the endoscope. In this regard, the GUPP consists of a wheeled base to provide platform mobility in the OT, and six serial passive joints for dexterous set-up. The backbone of the robot extends vertically from the underpan with a structure to enclose the electrical devices (on-board PC and DC power supply) and support the subsequent robot joints and structures. Here we denote the  $i$ th joint in GUPP by  $\mathcal{P}_i$  for a prismatic joint and  $\mathcal{R}_i$  for a revolute joint, respectively. The first joint  $\mathcal{P}_1$  is a non-back-drivable ball screw drive that moves parallel to the backbone subject to manual adjustment via a rod handler, which determines the robot height from 1830 mm to 2230 mm. In practice, the joint  $\mathcal{P}_1$  could be preset independently before entering the OT.

The subsequent joints of GUPP are described schematically by  $\mathcal{R}_2 - \mathcal{P}_3 - \mathcal{P}_4 - \mathcal{R}_5 - \mathcal{R}_6$ . The joint  $\mathcal{R}_2$  generates rotation along the vertical axis, while the joint  $\mathcal{P}_3$  is a linear guide that adjusts the horizontal distance of the RCM from the base. The combination of the first three joints  $\mathcal{P}_1$ ,  $\mathcal{R}_2$

TABLE I  
MOTION PROPERTIES OF THE SIX-DOF PASSIVE JOINTS

| Joint           | Min. pos. | Max. pos. | Unit     | Endoscope motion    |
|-----------------|-----------|-----------|----------|---------------------|
| $\mathcal{P}_1$ | -200      | 200       | mm       | vertical position   |
| $\mathcal{R}_2$ | -180      | 180       | $^\circ$ | horizontal position |
| $\mathcal{P}_3$ | -145      | 145       | mm       | horizontal position |
| $\mathcal{P}_4$ | -125      | 125       | mm       | vertical position   |
| $\mathcal{R}_5$ | -180      | 180       | $^\circ$ | yaw rotation        |
| $\mathcal{R}_6$ | -45       | 45        | $^\circ$ | pitch rotation      |

and  $\mathcal{P}_3$  forms an overhead cantilever crane that creates a staff-available space around the operating table. The prismatic joint  $\mathcal{P}_4$  provides vertical adjustment of the RCM with a 290 mm motion range, which contributes to a reachable height of RCM among 670-1310 mm above the floor. This fits the configuration where the patient is positioned for sinus surgery on a multi-purpose operating table [26]. The revolute joints  $\mathcal{R}_5$  and  $\mathcal{R}_6$  generate additional dexterity to adapt to the initial head orientation of the patient which varies from individual cases upon the surgeon's preference. The adjustable ranges of the six passive joints are indicated in Table I for reference.

#### B. Active Joint Set (AJS)

To provide a safe and dexterous motion workspace for the endoscope that yields the SPA, the AJS is designed, installed on the last link of the GUPP via an adapter unit, to generate a mechanically constrained RCM with three motorized joints (described by  $\mathcal{AR}_1 - \mathcal{AR}_2 - \mathcal{AP}_3$  schematically, refer to Fig. 2(b)). Note that the active DoF for lens shaft rotation has been deducted compared to the prototype in [35], [37] as the adjustment is preferred by the surgeon manually for ease of control. The joint  $\mathcal{AR}_1$  outputs rotational motion along the vertical axis from the motor via a worm drive and a synchronous belt for speed reduction within a compact joint case. For space clearance around the nostril (or the RCM), a curvilinear gear rack is installed inside a U-shape groove on  $\mathcal{AR}_2$  by two pairs of guiding rollers.

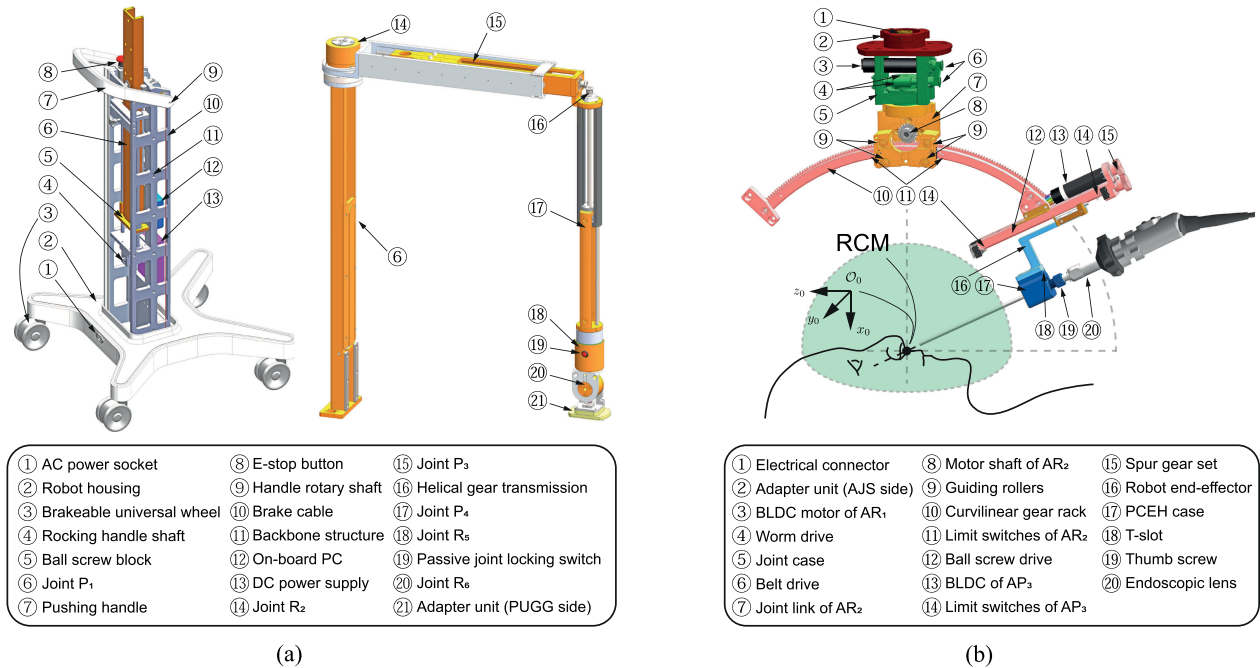


Fig. 2. (a) Mechanical design of the robot base and passive joints in GUPP. (b) Structure of the AJS with the mounted PCEH at the end-effector. The volume marked in green indicates the released space to facilitate coaxial instrument manipulation for manual procedures.

TABLE II  
MOTION PROPERTIES OF THE THREE-DOF ACTIVE JOINTS

| Joint  | Min. pos. | Max. pos. | Unit | Endoscope motion        |
|--------|-----------|-----------|------|-------------------------|
| $AR_1$ | -180      | 180       | °    | Frontal plane rotation  |
| $AR_2$ | -5        | 42        | °    | Sagittal plane rotation |
| $AP_3$ | -15       | 85        | mm   | Shaft translation       |

The structure enforces the curvilinear gear rack to rotate circumferentially around its center of curvature (i.e., the RCM). A prismatic motion is additionally provided by  $AP_3$  with a ball screw drive whose joint axis coincides with the endoscopic lens shaft. The joint  $AR_1$  and  $AR_2$  rotate the endoscope along the frontal plane (yaw motion) and sagittal plane (pitch motion), respectively, elevated when the positions of the revolute joints in GUPP are set to zeros. The joint  $AP_3$  is responsible for the insertion/retraction of the endoscope into/from the patient's nasal cavity. The motion properties of the active joints (see Table II) are defined, validated in our cadaver study, based on the result in [26]. Denote the joint positions of  $AR_1$ ,  $AR_2$  and  $AP_3$  by  $q_1$ ,  $q_2$  and  $q_3$  respectively, the joint space of the AJS is then described by

$$\mathbf{q} = [q_1 \ q_2 \ q_3]^T. \quad (1)$$

To analyze the forward kinematics of the AJS, we assign the base frame  $\mathcal{F}_0(\mathcal{O}_0, x_0, y_0, z_0)$  whose origin  $\mathcal{O}_0$  is identical to the RCM (see Fig. 2(b)), the x-axis and z-axis are parallel to the joint axes of  $AR_1$  and  $AP_3$ , respectively, while the joint angles of AJS are all zeros. The structure also enforces the lens body to pass the RCM when  $q_3 = 0$  to maintain the functionality of

RCM towards SPA. The use of the adapter unit allows different AJSs to be customized compatible to the same GUPP for various robot-assisted procedures.

### C. Passive-Compliant Endoscope Holder (PCEH)

RAEM owns risk of patient-side tissue damage in case of misoperations since the cluttered nasal cavity only tolerates limited space for instruments [36]. We design a novel PCEH at the end-effector of the AJS to bridge the connection between the endoscope and the robot structure with passive compliance. The internal structure of the PCEH is illustrated in Fig. 3(a). The PCEH is composed of a T-shape block which is fixed on the guide plate of  $AP_3$ , and a matching T-slot structured on the holder case, which suggests PCEH is pluggable for independent sterilization and can mount different customized holders. The passive compliance of the holder is achieved by a universal joint with tension spring I mounted circumferentially around it, from which the lateral tension forces and motions relative to the lens shaft is provided. The inner end of the universal joint is a friction block in contact with a friction plate fixed on the holder case. The shaft hub I is installed on the other side of the friction plate to constrain the insertion direction of the lens such that it goes through the hollow shaft of the universal joint, where another tension spring II is circumferentially mounted to provide axial tension force for compliance along the lens shaft. The surgeon could constrain the lens rotation along its shaft by manually tightening a thumb screw on the clamp shaft collar. The materials for compliant joint and shaft hub are stainless steel, and aluminium alloy with oxide layer for the joint case. This makes PCEH sterilizable by autoclaving. The PCEH is

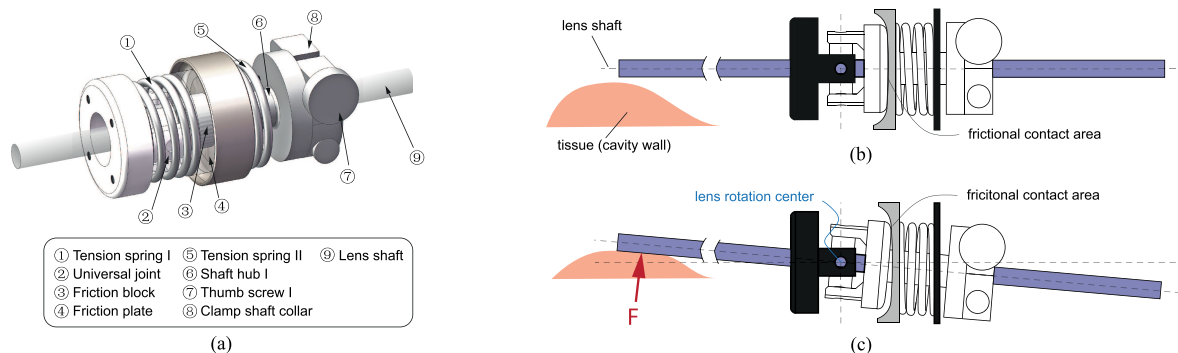


**Fig. 3.** (a) Structural design of the PCEH. (b) The PCEH working in rigid state with the tension spring I omitted for better visualization. The universal joint position is at its original position. (red area as the cavity wall, purple as the endoscopic lens, dark gray as components that are fixed with PCEH joint case, light gray as the friction plate which is movable along the shaft direction). (c) The PCEH working in the compliant state, where a large equivalent concentrated force  $F$  overcomes the static frictional force generated by the friction plate, resulting in relative motion at the frictional contact area. The lens is further rotated about the universal joint center. The reduced area relative to it in (b) guarantees small interaction force to not fracture the tissue.

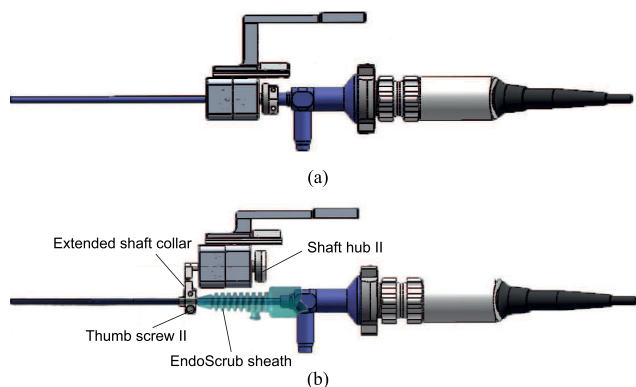


**Fig. 4.** (a) Lens installation without the sheath using shaft hub I. (b) Lens installation with the sheath using extended shaft collar and shaft hub II.

available to endoscopes with sizes of 4 mm and 2.7 mm which are respectively for adult and pediatric use in FESS.

The PCEH has two working states: the rigid state and the compliant state. Naturally, the holder works in the rigid state (shown in Fig. 3(b)), where the universal joint stays at its original position and the lens shaft is parallel to the centerline of the PCEH structure. The endoscope generates rigid motions together with the robot end-effector, which is helpful for steady endoscope positioning against inevitable physical interactions with other surgical instruments. On the other hand, an excessive (transverse) external force applied to the lens (happens when the lens collides with the cavity wall) will force a relative motion between the friction plate and block. The universal joint will be passively rotated with respect to its geometric center together with lens, inducing the latter to move away from the RCM and gives way to the contacted tissue (illustrated in Fig. 3(c)). At this stage, the PCEH passively switches to the compliant state. Such property stays until the universal joint reaches the maximum rotation angle of  $10^\circ$ , corresponding to a 26 mm displacement from the mounted lens tip (measured using the Karl Storz 7200 A endoscopic lens). Although such displacement is capable for surgeon-side perception, manual

**TABLE III**  
MECHATRONIC PERFORMANCES OF THE THREE-DOF ACTIVE JOINTS

| Metric                | $\mathcal{AR}_1$    | $\mathcal{AR}_2$    | $\mathcal{AP}_3$ |
|-----------------------|---------------------|---------------------|------------------|
| Motor gearbox ratio   | 157:1               | 86:1                | 84:1             |
| Joint reduction ratio | 40:1                | 22.5:1              | 1:1              |
| Motor steps/Rev.      | 6                   | 24                  | 6                |
| Min. pos. step        | $0.010^\circ$       | $0.008^\circ$       | 0.333 mm         |
| Preset motor speed    | $\pm 3000$ rpm      | $\pm 400$ rpm       | $\pm 6000$ rpm   |
| Preset joint velocity | $\pm 2.866^\circ/s$ | $\pm 1.240^\circ/s$ | $\pm 2.381$ mm/s |

recovery from collision is still required by the surgeon until the PCEH returns to the rigid state automatically. The threshold value of the external force that triggers the compliant state is influenced by the maximum static frictional force between the friction plate and friction block, which will be evaluated in Section V-A.

In clinical practice, the surgeon needs to install a sheath that covers the lens to drain the normal saline for lens tip cleaning with no need of withdrawing the endoscope from the nasal cavity. This is satisfied by our system using shaft hub II (shown in Fig. 4(b)) to install the endoscope parallel to the PCEH. An extended shaft collar is used to provide space for the sheath around the holder case. The availability of the RCM and passive compliance are both retained.

## IV. MECHATRONIC AND SOFTWARE DESIGN

### A. Control Architecture

The passive joints on the GUPP from joint  $\mathcal{R}_2$  to  $\mathcal{R}_6$  are equipped with self-locking brakes as fail-in-safety protection. The electromagnetic brakes provide either full brake engaging or releasing to joint positions, using a (normally open) switch on the link of joint  $\mathcal{P}_4$ . As the joint  $\mathcal{P}_4$  has a back-drivable ball screw drive for manual adjustment, we connect the screw shaft with a DC motor to compensate the gravity load of the subsequent structures to enable safer and easier manual adjustment. The motorized joints in AJS are actuated by brushless DC motors with the controllers installed on respective links as on-board connections. The active joints are non-back-drivable due to high

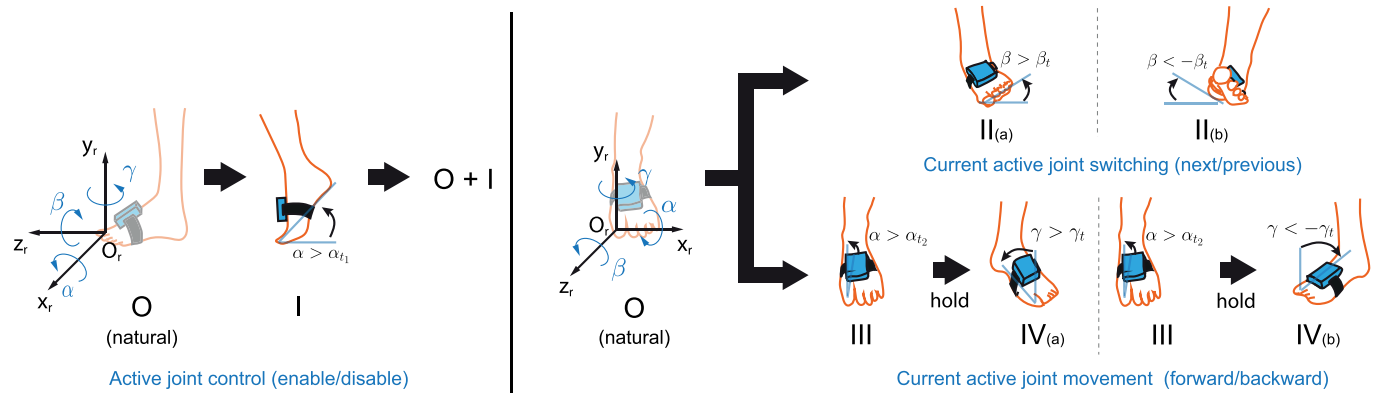


Fig. 5. Illustrated sets of foot gestures (I/II/III+IV) to foot-control the FREEDOM (demonstrated as left-foot mounted).

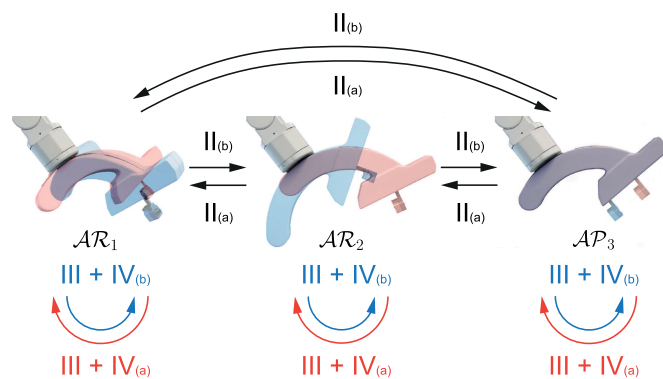


Fig. 6. Illustration of the foot gestures and their corresponding actions for intraoperative control of the active joints. Red/Blue arrows and the composite red/blue joint visualizations indicate backward/forward joint motions.

reduction ratios ( $>84 : 1$ ). Hall sensors are integrated to the motors in the AJIS for joint position measurements.

The controllers connect from joint  $\mathcal{P}_4$  (as the master controller) to joint  $\mathcal{AR}_1$ ,  $\mathcal{AR}_2$ , and  $\mathcal{AP}_3$  (as the slave controllers) via CAN-bus communication. To protect the mechanical structure of the AJIS, hardware limit switches are installed for joint  $\mathcal{AR}_2$  and  $\mathcal{AP}_3$ , with the position limit of joint  $\mathcal{AR}_1$  being detected in software level. Escaping from extreme joint positions are automatically triggered. The mechatronics for the active joints are listed in Table III. The controllers and the electromagnetic brakes are supported by a 24 VDC medical-use power supply. An E-stop (normally closed) button is placed such that it freezes all robot joints at their current positions once engaged. The controllers are commanded by an on-board PC integrated to the GUPP of the robot with the communication baud rate at 1 Mbit/s. The framework of the software control program is based on C++ running on Windows operating system.

## B. Foot-Wearable Interface

In FESS, concentration of the staff at the operating table may reduce the reliability of voice recognition or marker-based visual tracking for robot control purpose. To relieve both the endoscope handling and interface control from the surgeon's

hand, a foot-wearable control interface is designed to achieve FREEDOM control by means of surgeon's foot gestures, whose basic functionality has been partially presented in [37]. The interface is mounted on the back of the surgeon's single foot via an elastic band wrapping around the sole. An inertial measurement unit (IMU) detects the user's 3-DoF relative foot orientation over time. The device is battery-powered and supports Bluetooth communication between the interface microprocessor and the on-board PC.

Assigning a coordinate frame  $\mathcal{F}_f(\mathcal{O}_f, x_f, y_f, z_f)$  in Cartesian space that rotates with the foot over time with respect to its initial (referenced) pose  $\mathcal{F}_r(\mathcal{O}_r, x_r, y_r, z_r)$ . Thus, the foot rotation (denoted by  ${}^r\mathbf{R}_f$ , from  ${}^r\mathbf{p} = {}^r\mathbf{R}_f^f\mathbf{p}$  with  $\mathbf{p}$  being a 3D point in Cartesian space) can then be characterized by Euler angles  $\alpha$ ,  $\beta$ , and  $\gamma$  corresponding to the axes  $x_r$ ,  $y_r$ , and  $z_r$ , respectively, which are directly measurable using the IMU. To detect the changes of Euler angles from its original ones (i.e., equal to zeros) for gesture recognition purpose, we define the following thresholds:

$$[\alpha_{t_1} \ \alpha_{t_2} \ \beta_t \ \gamma_t] = [55^\circ \ 15^\circ \ 20^\circ \ 20^\circ] \quad (2)$$

which are determined upon satisfaction of foot reachability and pose-wise distinguishability according to our surgeons. The rotating angle for each DoF is continuously measured, with the noise from the raw sensing data being dealt with by a first-order low-pass filter. Surpassing the corresponding threshold by either DoF will directly be detected by the algorithm for gesture recognition without further processings.

A set of pre-programmed foot control gestures are designed for the surgeon to issue different control commands for RAEM (illustrated in Fig. 5). The surgeon could enable/disable the foot control towards the robot by using Gesture I, i.e., plantar flexion (until  $\alpha > \alpha_{t_1}$ ) twice within two seconds, from which in disabled mode the surgeon could move the foot freely without risks of accidental activation. The Gesture II(a/b), defined by inversion/eversion of the wearing foot (with  $|\beta| > \beta_t$ ), changes the current-selected active joint schematically/anti-schematically. When the interface control is enabled, moving the current joint along positive/negative direction is done by keeping plantar flexion (Gesture III, with  $\alpha > \alpha_{t_2}$ ) with toe rotation clockwise/anti-clockwise (Gesture IV(a/b), with  $|\gamma| > \gamma_t$ ). Here, enforcing the

TABLE IV  
CORRESPONDENCES OF VOICE INDICATIONS AND TRIGGERING  
GESTURES/EVENTS

| Joint      | Gesture  | Purpose/Event       | Verbalization           |
|------------|----------|---------------------|-------------------------|
| $AR_1$     | III      | To check joint      | “Horizontal”            |
|            | II(a/b)  | To switch joint     | “Zooming”/“Vertical”    |
|            | III+IV   | To move joint       | “Left”/“Right”          |
| $AR_2$     | III      | To check joint      | “Vertical”              |
|            | II(a/b)  | To switch joint     | “Horizontal”/“Zooming”  |
|            | III+IV   | To move joint       | “Up”/“Down”             |
| $AP_3$     | III      | To check joint      | “Zooming”               |
|            | II(a/b)  | To switch joint     | “Vertical”/“Horizontal” |
|            | III+IV   | To move joint       | “In”/“Out”              |
| $\times^*$ | I        | To toggle control   | “Enable/Disable”        |
|            | $\times$ | Joint limit reached | “Reaching limit”        |
|            | $\times$ | E-stop pressed      | “Emergency stop”        |

\*The  $\times$  means the event is independent of the status in the current term.

combined use of Gesture III and IV could prevent robot from being activated by unguarded foot motions of the surgeon. No airborne actions are required to the controlling foot for ease of maintaining the surgeon’s body balance. The interface could be worn by the surgeon on either foot.

Improvements have been made to the algorithm from our previous one [37] for better performance. According to the introduced algorithm, the natural standing orientation of the controlling foot (which serves as the referenced pose for detection) should not be greatly changed (e.g.  $\gamma > 90^\circ$ ). This might restrict the surgeon from freely changing his/her standing position intraoperatively. To deal with this, we develop to automatically register the reference frame  $\mathcal{F}_r$  if the sole of the foot sticks continuously to the ground for a certain period (i.e.,  $|\alpha| \approx 0$  for 2 s). This could enhance the robustness of foot gesture detection for recognition. Another practical problem to the surgeon is that leaving the endoscope static for a long-term procedure may lead to forgetting the currently-controlled DoF. We solve this issue by further developing a voice indication algorithm based on Speech Application Programming Interface (SAPI, by Microsoft). The algorithm is embedded to the interface control loop and could verbalize the current working status (including the current DoF, moving direction, joint limit warning, etc.) Except the joint limit warning (automatically announces when the event is triggered), indications of the joint status are generated according to the surgeon’s foot gestures and the current DoF (see indication correspondences Table IV). This helps the surgeon be aware of the output motion to reduce risks of misoperations. Fig. 7 gives the full control strategy of the surgeon to perform robot-assisted FESS using the FREEDOM. The scheme emphasizes a surgeon-centered configuration that the surgeon could manipulate the endoscope via the control interface while performing bimanual operations.

## V. RESULTS

### A. Fabricated Prototype

The net weight of the FREEDOM is 45.5 kg (compared to the  $\sim 800$  kg dVSS). The robot housing is made from PVC material to minimize the exposure of metallic structures for enhanced electrical safety and to provide a less obtrusive appearance of

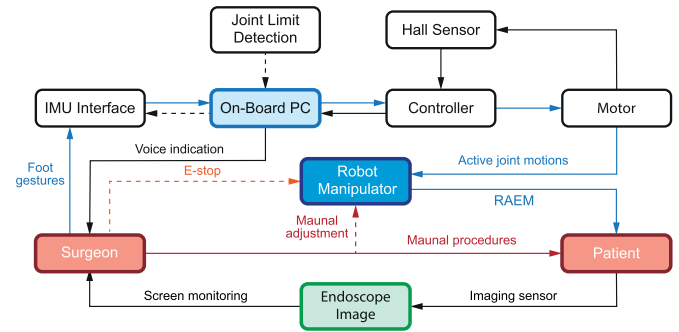


Fig. 7. The control diagram of the FREEDOM for RAEM in FESS. The surgeon manipulates the endoscope either using the AJS or GUPP via foot control or manual adjustment, respectively. Meanwhile, the surgeon performs manual procedures using two hands.

the prototype inside the OT. All electrical components including the on-board PC and the robot controllers are embedded to the GUPP, enabling a single cable set-up (the 220 V-50 Hz AC power input) process. The robot’s working status and online data could be monitored via remote control from the on-board PC using WLAN communication. Thus, physical connections from external devices to the system are prevented to improve the electrical safety as well. Of note, the prototype satisfies the general standard IEC 60601-1 for medical-grade electrical safety, which is essentially required for the system to enter the OT.

### B. Laboratory Study

1) **Endoscope Positioning:** In this section, we demonstrate the performance of the FREEDOM to multiple laboratory experiments. The positioning error for the endoscope lens tip in 3D space appeared in the control process is tested. The performance is evaluated with all the passive joint positions in GUPP set to zeros. The mean positioning error is 2.6 mm (range 0.4–3.2 mm) within the whole workspace of AJS, mainly due to mechanical backlashes and/or calibration between the hall sensors and the joint positions. Meanwhile, the high absolute accuracy is not critically required by the FREEDOM since the surgeon-in-the-loop configuration. The minimum motion steps that the active joints provide for endoscope positioning can be referred to Table III.

2) **Performance of the PCEH:** Lens-tissue collisions may occur at different positions along the lens inside the cavity. To test the force values that trigger the compliant state of the PCEH, external forces applied from different directions, and also, towards different positions of the lens are tested to evaluate its safety performance. The Karl Storz 7200 A 4 mm–30° endoscopic lens is installed on the PCEH without using the lens sheath. The rear part of the endoscope (comprising the camera sensor and the connected wires) along the direction  $-\mathcal{O}_0x_0$  generates a 1.43 N force with the gravity center positioned at  $(0, 0, -92)^T$  mm which will be added to our online-measured data. A 6-DoF force sensor (ATI SI-80-4, resolution 0.04 N) is used to measure the interacting force. The sensor is to be pushed towards the lens shaft along the transverse direction (i.e.

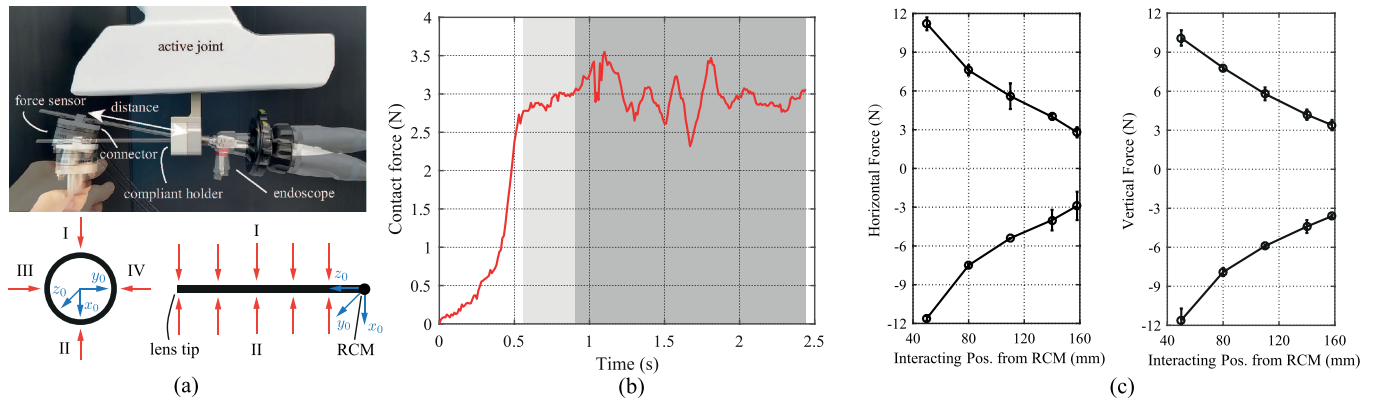


**Fig. 8.** (a) The experimental set-up for compliant force test for PCEH, with the tested forces to be applied from the four directions ( $+\mathcal{O}_0x$  as I,  $-\mathcal{O}_0x$  as II,  $+\mathcal{O}_0y$  as III,  $-\mathcal{O}_0y$  as IV) transversely towards the lens, viewing from the axial direction, and the contact positions to the lens body (red arrows conceptually indicate the applied forces). (b) The measured contact force with 158 mm along  $+\mathcal{O}_0z_0$ , the measured threshold force value is 2.8 N measured at  $t = 0.52$  s (the light/dark gray area indicates that the PCEH works in compliant state with the lens moving/stopped). (c) The mean threshold force values to trigger the PCEH's compliant state under different positions on the lens. Ten experiments are done for each interacting position and direction.

along the negative  $z$ -axis for the sensor) manually via a handler to simulate the forces resulted from lens-tissue interaction (see Fig. 8(a)). Forces from four directions (two horizontal as  $+\mathcal{O}_0y_0$  and  $-\mathcal{O}_0y_0$ , two vertical as  $+\mathcal{O}_0x_0$  and  $-\mathcal{O}_0x_0$ ) are applied respectively to study the homogeneity of the threshold forces via different directions (see illustration in Fig. 8(a)). At each direction, five sensor-lens interaction points with different distances from the RCM point along  $+\mathcal{O}_0z_0$  are further selected as depicted in Fig. 8(a). Fig. 8(b) shows the force data from one test (contact point 158 mm along  $+\mathcal{O}_0z_0$ ). The contact force rises dramatically under rigid state and levels off during the compliant state. Stopping the sensor displacement stabilizes the mean value of force around the threshold (2.4–3.5 N) due to hand tremor. Furthermore, the results plotted in Fig. 8(c) show that smaller thresholds are recorded due to farther interacting positions from the RCM. When the collision happens close to the lens tip (the usual interaction position in FESS), the mean threshold force is 3.0 N (range 2.8–3.2 N) from the four tested directions. Note importantly that the results from 17 nasal cavities in our cadaver tests showed that the mean force value to fracture the lamina papyracea is 6.0 N. Therefore, the compliant state of PCEH could be triggered to effectively protect the tissue from damage. Safe compliance (contact force  $< 6.0$  N) is further provided when the contact point of the lens is around 100–158 mm along  $+\mathcal{O}_0z_0$  from the RCM. The importance of such compliance is to create buffer time for the surgeon to perceive the lens-tissue collision, such that he/she could take immediate actions.

**3) Foot-Controlled Endoscope Manipulation:** A laboratory-based RAEM procedure for FESS using the proposed interface is conducted to test the foot control method. The set-up comprises a human head model for ENT surgery training, a monocular endoscope device set (with a 4 mm lens, an imaging sensor and a lighting source) and a desktop monitor that visualizes the images. The interface is mounted on the right foot of an experienced user to control the insertion/retraction of the lens through the nostril. The threshold angles to recognize the plantar flexion and toe rotation are set to  $20^\circ$  and  $\pm 20^\circ$ ,

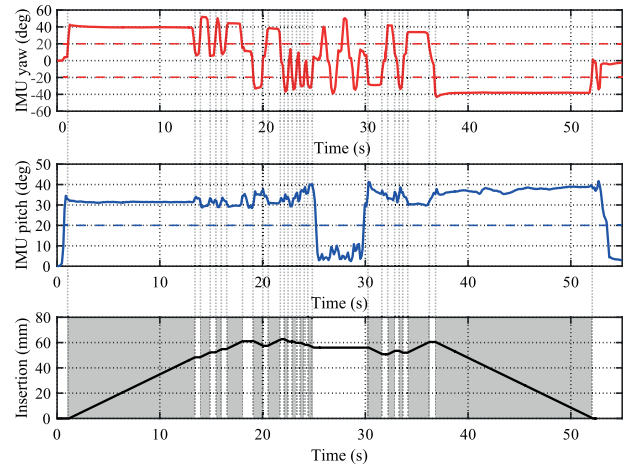


**Fig. 9.** The joint position of  $\mathcal{AP}_3$  subject to control by the foot interface. In the time periods marked in gray, the joint is being moved by foot-controlled commands. The movement indicates a full insertion (0–13 s) and full retraction (37–52 s) of the lens inside the model's nasal cavity with fine field-of-view adjustment (13–37 s).

respectively, as suggested by the surgeon. The interface control loop is 43 ms without processing optimization for real-time mastering by the surgeon.

The data illustrated in Fig. 9 demonstrates the triggering motions of  $\mathcal{AP}_3$  upon user's control. The user finishes four steps of RAEM: 1) Endoscope insertion into the nasal cavity (2–18 s); 2) local adjustment of lens (20–25 s); 3) standing position adjustment; 4) endoscope retraction (37–52 s). The gray areas continually appeared from the insertion data in Fig. 9 are the time periods when the joint motions were activated. The user was able to complete frequent joint motion control for fine endoscope adjustment (22–25 s). The gestures are recognizable by the IMU sensor since the pre-set thresholds are well surpassed ( $> 10$  degrees, as shown in Fig. 9(a)(b)). With the ground-touching sole, the interface rejected orientation disturbance that does not trigger the robot accidentally (25–30 s).



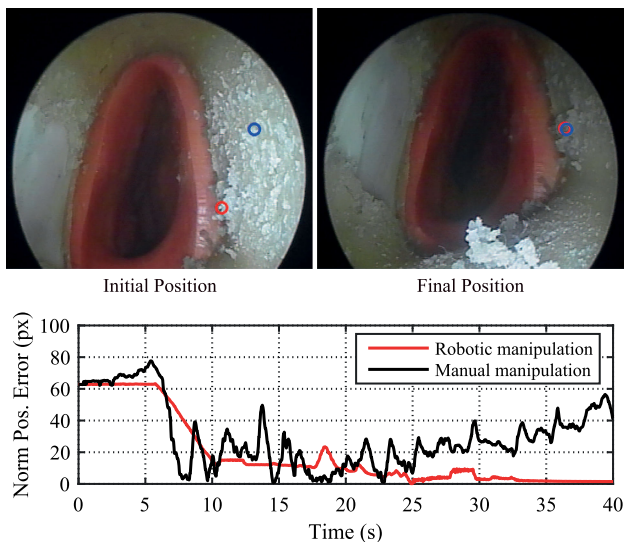


Fig. 10. Results of manual/robot-assisted endoscope manipulation based on image features (red circle as tracking point, blue circle as (static) target point).

An endoscope positioning procedure is further conducted to evaluate the effectiveness of RAEM. A world feature point inside the nasal cavity model is selected and tracked via optical flow (Kanade-Lucas-Tomasi) method (see Fig. 10 for details). The user is expected to coincide the projected 2D feature point towards a target 2D position on the image, which is used in regular FESS for inspection of certain surgical areas upon field-of-view adjustment. Both manual and robot-assisted endoscope manipulation are performed with a 4mm-0° endoscope lens. The position errors between the feature and the 2D target on the image are shown in Fig. 10, performed by a proficient user. The manipulating velocity is constrained to 1.5 mm/s to keep the tracking algorithm effective. The error is significantly decreased under manual handling, followed by the decrease of error under RAEM. However, robotic manipulation leads to enhanced handling stability, compared to the drifted point tracking result caused by hand tremor from manual handling when  $t > 25$  s.

### C. Cadaver Experiments

The feasibility study of the FREEDOM in the OT for RAEM should be evaluated prior to clinical-stage applications. In this regard, we have conducted cadaver experiments to test the system viability in the OT during the surgery.<sup>2</sup> Four fresh cadaver heads with a total of eight nasal cavities were performed identical FESS procedures including maxillary antrostomy, total ethmoidectomy, and sphenoidotomy. There were no significant disparities among individual cadavers that might affect the difficulty for the surgeon to perform FESS. Each cadaver head was placed on the operating table secured with headrest blocks for ease of performing the surgery. The robot base was localized at

<sup>2</sup>The cadaver study were conducted at the CUHK Jockey Club Minimally-Invasive Surgical Center, Prince of Wales Hospital, HKSAR, China.

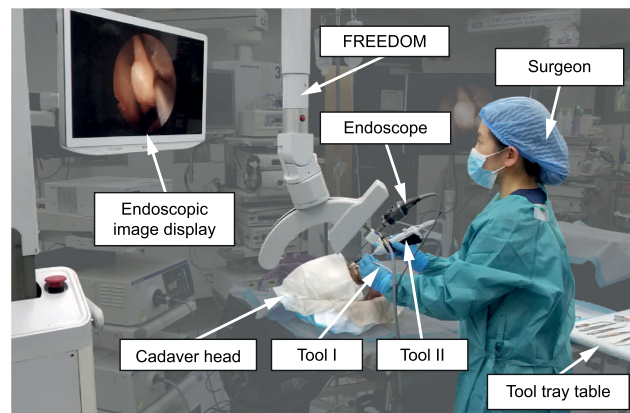
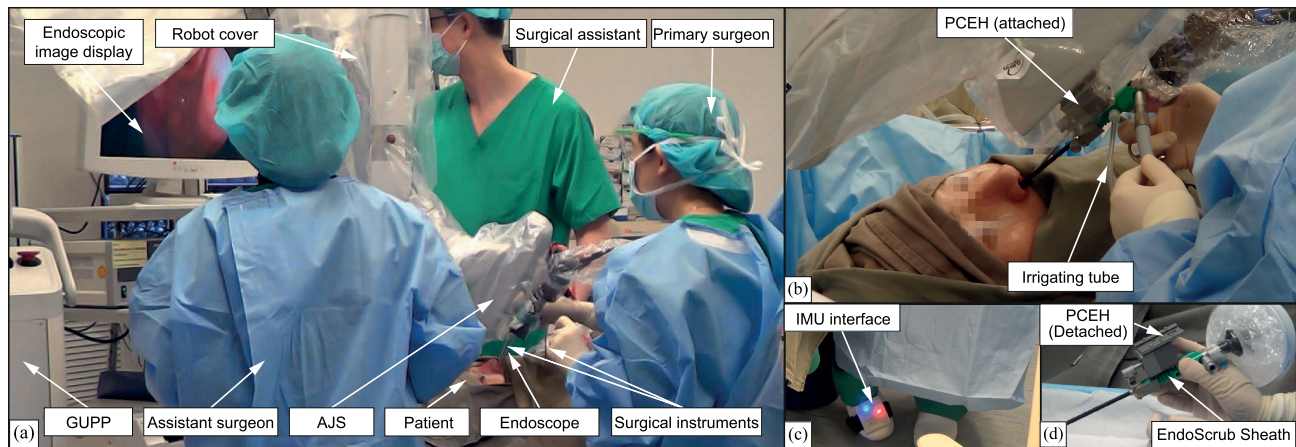


Fig. 11. Robot set-up for cadaver study. With RAEM, the surgeon was able to manipulate two tools (tool I for blood suctioning and tool II for tissue cauterization) using respective hands during FESS.

TABLE V  
CUMULATIVE MOVING TIMES AND DURATIONS OF ACTIVE JOINTS IN EACH CADAVER CASE

|         | Term         | $AR_1$ | $AR_2$ | $AP_3$ | Sum   |
|---------|--------------|--------|--------|--------|-------|
| Case #1 | Times        | 74     | 97     | 94     | 265   |
|         | Duration (s) | 58.3   | 104.8  | 127.3  | 290.4 |
| Case #2 | Times        | 38     | 44     | 62     | 144   |
|         | Duration (s) | 33.4   | 45.0   | 83.2   | 161.6 |
| Case #3 | Times        | 32     | 17     | 44     | 93    |
|         | Duration (s) | 22.4   | 29.8   | 71.7   | 123.9 |
| Case #4 | Times        | 41     | 31     | 46     | 118   |
|         | Duration (s) | 36.6   | 45.8   | 53.5   | 135.9 |

the superior position of the patient. The mean set-up time for each cadaver head was 2.6 mins (range 1.6–4.4 mins). During the FESS, one surgical staff was responsible to prepare a tray table located next to the surgeon with surgical instruments on it. Bimanual operations and instrument switching were done without help from the surgical staff. Fig. 11 demonstrates the surgeon performing robot-assisted FESS using the FREEDOM alone. The surgeon continually used the interface to adjust the field of view of the endoscope by RAEM. The used motion ranges of the active joints are recorded from the FESS to eight nasal cavities, with  $-30^\circ$ - $33^\circ$  for  $AR_1$ ,  $0^\circ$ - $23^\circ$  for  $AR_2$ , and  $-8$  mm-41 mm for  $AP_3$ , all satisfying the designed ranges in Table II. The number of times that the active joints were triggered with the cumulative moving time during each case (i.e., FESS to two nasal cavities) were recorded in Table V. The data indicates that inserting/retracting the endoscope (driven by the  $AP_3$ ) was performed most frequently during FESS, which was a more spatially available DoF inside the cavity for position adjustment. The mean net duration for adjusting the endoscope in each case was 2.97 mins (range 2.1–4.8 mins), while the surgeon concentrated on the surgical procedures relying on static endoscope positioning most of the time. Notably, the cumulative number of times and durations for control decreased significantly as the surgeon gained proficiency through four individual cases. The functionality of the FREEDOM has been successfully validated, which is a crucial step to further explore its clinical merit.



**Fig. 12.** Clinical study of robot-assisted FESS on human patients using the FREEDOM for endoscope manipulation. (a) The locations of the primary surgeon, the assistant surgeon, the surgical staff and the FREEDOM in the OT. The surgeon was able to hold two different instruments using respective hands most of the time during the surgery. (b) A close-up view towards the surgery details. The available space around the nostril facilitated co-axial instrument manipulation as it in regular routine. (c) The foot interface was worn by the primary surgeon's right foot for controlling the endoscope. (d) The installed endoscopic lens on the PCEH with the lens sheath covered during set up.

#### D. Clinical Trials: Robot-Assisted FESS

Having validated the basic functionality of the FREEDOM via *ex-vivo* cadaver experiments, the next phase of our study is to assess its surgical applicability via clinical investigation. The FREEDOM prototype is to be placed inside the OT to participate in regular FESS procedures, from which intraoperative data (operating time, robot performance, etc.) is collected to evaluate its immediate adaptation to the surgery. We present results of our study in two patients so far who had been performed robot-assisted FESS.<sup>3</sup>

**1) Participants and Surgeons:** The inclusion criteria for choosing participants were: 1) patients who were 18 years old or older; 2) patients who had benign pathology and would undergo FESS to improve sinus ventilation after failing medical treatments. In our two cases, one patient was to be performed right sinus operation, with the other the left and right sinus operation. The cases were conducted by the same primary surgeon who was an expert in FESS. The surgeon was trained (including  $\sim 10$  mins of lab training and  $\sim 4$  mins of on-site training) to be capable of using the control interface independently for intraoperative mastering of RAEM.

**2) System Preparation and Set-Up:** The distal structure of the FREEDOM (starting from joint  $\mathcal{P}_3$ ) was enclosed by a medical equipment cover to prevent contamination. The detachable part of the PCEH had been sterilized via autoclaving and was prepared for the case by surgical staff alongside other surgical instruments. Following the patient coming into the OT, the surgical staff set up the system following the schematic objectives below:

- i) The robot base was docked at the rear position next to the patient's head with the in-between space enabling staff to walk through.

- ii) The passive joints  $\mathcal{P}_1 - \mathcal{P}_4$  in GUPP were adjusted to move the position of the RCM adjacent to the nostril.
- iii) The passive joints  $\mathcal{R}_5 - \mathcal{R}_6$  in GUPP were adjusted to further set up the initial orientation of the endoscope.
- iv) The lens was mounted, with the EndoScrub lens sheath covered, to the detachable part of the PCEH. The latter was then further installed to the robot end-effector.
- v) Fine pose tuning for final settlement of the endoscope was done according to the surgeon's individual preference.

The preoperative set-up was considered completed as: 1) the RCM position was coincided with the interested nostril, and 2) the lens shaft insertion direction was aligned with the centerline of the nasal passage. The settlement was made upon surgeon's empirical judgment.

**3) Workflow:** The surgeons stood in their regular positions at the head of the patient who was under general anaesthesia. The endoscope was inserted into the patient's nasal cavity via foot control by the surgeon until obtaining good visibility and maximal accessibility to the surgical (sinus) area. Visualization was provided by a Karl Storz Image 1 H3-Z telescope camera with Hopkins 7200 A 4 mm-0°/30° rod lens. Coaxial manipulation of surgical instruments through the nostril was done by the surgeon side-by-side leaving the workspace unobstructed by the AJS. Of particular note, the use of FREEDOM was proved by our study to enable the surgeon to perform the following THPs in FESS alone (see Table VI):

- *Maxillary antrostomy:* The surgeon medialized the middle turbinate, excised the uncinate with a sickle knife with one hand and widened the antrostomy with the other simultaneously.
- *Ethmoidectomy:* The surgeon performed tissue manipulation and dissection using respective hands simultaneously, with the lamina papyracea clearly defined.
- *Nasopharyngeal tumor resection:* The surgeon performed tissue dissection and retraction using respective hands simultaneously.

<sup>3</sup>The trials were conducted at the Prince of Wales Hospital, HKSAR, China.

TABLE VI  
SUMMARY OF ROBOT-ASSISTED FESS PROCEDURES USING THE FREEDOM IN OUR CLINICAL TRIALS

| Subject | Procedures   | GUPP set-up duration | Surgery duration | AJS unactivated duration | AJS activated duration | AJS activated times | Lens cleaning times | PCEH triggering times | Surgery Success |
|---------|--|----------------------|------------------|--------------------------|------------------------|---------------------|---------------------|-----------------------|-----------------|
| 1       | Right maxillary antrostomy<br>Nasopharyngeal tumor resection | 3.9 mins             | 108.1 mins       | 96.1 mins                | 1.9 mins               | 75                  | 4                   | 0                     | Yes             |
| 2       | Right maxillary antrostomy<br>Right ethmoidectomy            | 3.2 mins             | 79.3 mins        | 72.7 mins                | 1.7 mins               | 49                  | 2                   | 0                     | Yes             |

- *Bleeding treatment:* The surgeon did the blood suctioning and cauterization using respective hands simultaneously.

The endoscope was adjusted via foot-controlled AJS mostly. The GUPP was concurrently used in tasks involving RCM adjustment, such as retracting the endoscope for lens change or switching it between nostrils.

**4) Robot-Assisted Versus Regular FESS:** Robot-assisted FESS using the FREEDOM facilitated an improved surgeon-centered configuration. Surgical field observation was durably stabilized using RAEM with more precise adjustment, which further reduced the risk of colliding with the cavity wall (more common for hand-held). Meanwhile, as a result of reducing human workload with better performance, the surgeon highly relied on the static endoscope positioning provided by RAEM up to about 90% of the total surgery duration (i.e., the inactivated/activated duration data in Table VI). Using the FREEDOM also allowed the surgeon to handle two instruments using both hands (compared to the regular routine involving two surgeons). The endoscope was adjusted by the surgeon directly using the interface without using hands.

On the other hand, the success in clinical trials had proved that the routine (manual) FESS procedures went on smoothly with the FREEDOM. The surgeon's standing position, viewing condition of the endoscopic image display, and coaxial instrument manipulation space were not impinged by the robot structure. Cleaning the lens tip upon dripping blood and/or hazing was done, in the regular way, by irrigating the lens using normal saline via the EndoScrub lens sheath. The mean time cost for lens changing and re-installation (between 0° and 30° lens) was 1.5 mins. Special postoperative treatments were not required for the patients as exclusively resulted from RAEM.

The mean time to finish robot docking and set up of GUPP was 3.6 mins (range 3.2–3.9 mins). Of note, the control interface was also approached by another three surgeons who used it for the first time, with a mean learning curve of 3.4 mins (range 2.5–4.0 mins) recorded for each to independently master the foot control skills guided by an engineer.

**5) Surgeon-Side User Feedback:** The mean time to perform a maxillary antrostomy from medializing the middle turbinate, excising the uncinata with a sickle knife, to widening the antrostomy using RAEM was reasonable. The designed foot gestures maintained the surgeon's wearing foot contacting the ground which contributed to reduced distractions to the surgeon. Voice indication was preferred by the surgeon to obtain the status of the controlled active DoF without tentative endoscope movements. The interface was continuously used for 1.6 hours (full battery lasts > 4 hours) without additional

foot discomfort or fatigue compared to it in regular FESS. The estimated duration of robot-assisted FESS was 20% longer than regular FESS, stated by the surgeon. The compliant state of PCEH was not triggered during the clinical trials, but yet was important to provide additional safety under unexpected lens-tissue collision. Extensive statistical analysis will be conducted subject to increasing number of trials.

## VI. DISCUSSION AND CONCLUSION

In this paper, we report the design, development and clinical evaluation of a new robotic system FREEDOM for RAEM in sinus surgery. The passive-active combined joint set of the robot has provided a more stable and precise positioning platform free of hand tremor for the endoscope compared to manual handling. The PCEH has been introduced to reduce the risk of tissue fracture led by unexpected lens-tissue collisions. By providing the foot-wearable interface, the enabled hands-free endoscope adjustment becomes more surgeon-centered that is beneficial to hands-on procedures.

Four cadaver cases and two clinical trials were successfully conducted to provide proof of concept for the FREEDOM to assist FESS. The robot could be set up efficiently (mean 2.6/3.6 mins in cadaver/clinical studies) and the control interface owned a short learning curve (mean learning time 3.4 mins), adding no significant time for surgery preparation. It was clinically proved that, with side-by-side assistance using the FREEDOM, complicated THPs in FESS could be performed by the surgeon alone bimanually most of the time easily. The system did not disrupt the manual procedures and was generally not obstructive to the regular spaces required by the surgeon. No additional fatigue was reported by the surgeon in cadaver or clinical cases (continuous use up to 1.6 hours per case) for using the foot control interface. The work is believed to be the first FESS-customized robotic system which has been validated by clinical trials. The results have demonstrated the potential of FREEDOM to assist other endoscopic surgeries (e.g. ear and skull base surgery) which also involve endoscope-based THPs.

Despite positive results, limitations appear in the present version of FREEDOM. For example, the surgeon could only move one active joint at a time for endoscope adjustment. This increases the motion steps for endoscope adjustment and weakens its task efficiency. However, this is solvable by developing direct pose-to-pose adjustment method from foot pose variation to that of the endoscope. Another limitation relates to the response of the PCEH upon lens-tissue collision. Although the passive

compliance could prevent the tissue from fracture within certain a motion range, the surgeon is still required to perceive such situation to take immediate actions. Using sensor-based measurement (either force or rotary position detection of the compliant joint in the PCEH) could allow automatic escaping from lens-tissue collision. We are working on the issues brought by such solution to maintain the pluggable and sterilizable properties of the holder.

At current stage, the available data from limited number of cases is ample enough to demonstrate the system feasibility of the FREEDOM, but yet exhibits weak statistical significance. Comprehensive clinical data analysis will be conducted upon cumulative experimental data to further evaluate the clinical performance of the system. Meanwhile, existing results have provided supporting evidence for continuing development and updating of the FREEDOM system. We aim to tailor the foot gesture recognition to surgeons with different body habitus and/or foot agility by using self-learning detection thresholds. Future works also include exploration of various foot gesture sets with long-term user comfort evaluation, and the design of new PCEHs aiming for robot-assisted ear surgery using the identical GUPP.

#### ACKNOWLEDGMENT

The authors would like to acknowledge the staff from Prince of Wales Hospital for their support during clinical trials using the FREEDOM prototype. The ethics approval of this study is given by Joint CUHK-NTEC Clinical Research Ethics Committee (CRE Ref. No. 2017.307).

#### REFERENCES

- [1] S. Govindaraj *et al.*, "Endoscopic sinus surgery: Evolution and technical innovations," *J. Laryngol. Otol.*, vol. 124, no. 3, pp. 242–250, 2010.
- [2] A. Parmar *et al.*, "Robotic surgery in ear nose and throat," *Eur. Arch. Oto-Rhino-Laryngol.*, vol. 267, no. 4, pp. 625–633, 2010.
- [3] D. Kennedy, "Technical innovations and the evolution of endoscopic sinus surgery," *Ann. Otol., Rhinol. Laryngol.*, vol. 115, no. 9, pp. 3–12, 2006.
- [4] V. Trévilott *et al.*, "Robotic endoscopic sinus and skull base surgery: Review of the literature and future prospects," *Eur. Ann. Otorhinolaryngol., Head Neck Diseases*, vol. 130, no. 4, pp. 201–207, 2013.
- [5] G. Hager *et al.*, "Surgical and interventional robotics: Part iii: Surgical assistance systems," *IEEE Robot. Autom. Mag.*, vol. 15, no. 4, pp. 84–93, Dec. 2008.
- [6] M. Diana and J. Marescaux, "Robotic surgery," *Brit. J. Surgery*, vol. 102, no. 2, pp. e15–e28, 2015.
- [7] C. Coulson *et al.*, "ENT challenges at the small scale," *Int. J. Med. Robot. Comput. Assisted Surg.* vol. 3, no. 2, pp. 91–96, Sep. 2007.
- [8] R. Taylor, "A perspective on medical robotics," *Proc. IEEE*, vol. 94, no. 9, pp. 1652–1664, Sep. 2006.
- [9] R. Taylor *et al.*, "Medical robotics and computer-integrated surgery," in *Springer Handbook of Robotics*. Berlin, Germany: Springer, 2016, pp. 1657–1684.
- [10] P. Kazanzides *et al.*, "Surgical and interventional robotics-core concepts, technology, and design [tutorial]," *IEEE Robot. Autom. Mag.*, vol. 15, no. 2, Jun. 2008.
- [11] Z. Maan *et al.*, "The use of robotics in otolaryngology—head and neck surgery: A systematic review," *Amer. J. Otolaryngol.*, vol. 33, no. 1, pp. 137–146, 2012.
- [12] A. Arora *et al.*, "Clinical applications of telerobotic ENT-head and neck surgery," *Int. J. Surg.* vol. 9, no. 4, pp. 277–284, 2011.
- [13] J. Schneider *et al.*, "Robotic surgery for the sinuses and skull base: What are the possibilities and what are the obstacles?" *Current Opinion Otolaryngol. Head Neck Surg.* vol. 21, no. 1, pp. 11–16, 2013.
- [14] J. Hernandez *et al.*, "Qualitative and quantitative analysis of the learning curve of a simulated surgical task on the da Vinci system," *Surgical Endosc. Other Interventional Tech.*, vol. 18, no. 3, pp. 372–378, 2004.
- [15] J. Anon *et al.*, "Computer-assisted endoscopic sinus surgery: An international review," *Otolaryngologic Clin. North Amer.*, vol. 30, no. 3, pp. 389–401, 1997.
- [16] J. Wurm *et al.*, "A novel robot system for fully automated paranasal sinus surgery," in *Proc. Int. Congr. Series*, vol. 1256, pp. 633–638, Jun. 2003.
- [17] G. Strauss *et al.*, "Navigated control in functional endoscopic sinus surgery," *Int. J. Med. Robot. Comput. Assisted Surgery*, vol. 1, no. 3, pp. 31–41, 2005.
- [18] M. Rilk *et al.*, "Demonstration of a prototype for robot assisted endoscopic sinus surgery," in *Proc. IEEE Int. Conf. Robot. Autom.* 2010, pp. 1090–1091.
- [19] K. Eichhorn *et al.*, "Robot-assisted endoscopic guidance versus manual endoscopic guidance in functional endonasal sinus surgery (fess)," *Acta oto-laryngologica*, vol. 137, no. 10, pp. 1090–1095, 2017.
- [20] Z. Zeng *et al.*, "Approach and control for robot assisted sinus surgery," in *Proc. IEEE Int. Conf. Robot. Biomimetics*, 2017, pp. 983–988.
- [21] M. A. Obando and J. H. Payne, "The future application of the robotic arm (Automatic Endoscopic System for Optimal Positioning or AESOP) with voice recognition in sinus endoscopic surgery," *Operative Techn. Otolaryngol.-Head Neck Surg.* vol. 14, no. 1, pp. 55–57, 2003.
- [22] C. Nathan *et al.*, "The voice-controlled robotic assist scope holder AESOP for the endoscopic approach to the sella," *Skull Base*, vol. 16, no. 3, pp. 123–131, 2006.
- [23] J. Kristin *et al.*, "Development of a new endoscope holder for head and neck surgery from the technical design concept to implementation," *Eur. Arch. Oto-Rhino-Laryngol.*, vol. 272, no. 5, pp. 1239–1244, 2015.
- [24] J. Kristin *et al.*, "Assessment of the endoscopic range of motion for head and neck surgery using the SOLOASSIST endoscope holder," *Int. J. Med. Robot. Comput. Assisted Surg.* vol. 11, no. 4, pp. 418–423, 2015.
- [25] J. Burgner *et al.*, "A telerobotic system for transnasal surgery," *IEEE/ASME Trans. Mechatronics*, vol. 19, no. 3, pp. 996–1006, Jun. 2014.
- [26] V. Trévilott *et al.*, "Innovative endoscopic sino-nasal and anterior skull base robotics," *Int. J. Comput. Assisted Radiol. Surg.* vol. 8, no. 6, pp. 977–987, 2013.
- [27] X. Sun *et al.*, "Design of a robotic endoscope holder for sinus surgery," in *Proc. IEEE Int. Conf. Robot. Biomimetics* 2015, pp. 391–396.
- [28] C. Kunisaki *et al.*, "Video-assisted thoracoscopic esophagectomy with a voice-controlled robot: The AESOP system," *Surg. Laparoscopy Endoscopy Percutaneous Techn.* vol. 14, no. 6, pp. 323–327, 2004.
- [29] H. Yip *et al.*, "Development of an eye-gaze controlled interface for surgical manipulators using eye-tracking glasses," in *Proc. IEEE Int. Conf. Robot. Biomimetics*, 2016, pp. 1900–1905.
- [30] S. Ali *et al.*, "Eye gaze tracking for endoscopic camera positioning: An application of a hardware/software interface developed to automate AESOP," *Studies Health Technol. Inform.*, vol. 132, pp. 4–7, 2008.
- [31] J. Yamashita *et al.*, "Real-time 3-D model-based navigation system for endoscopic paranasal sinus surgery," *IEEE Trans. Biomed. Eng.*, vol. 46, no. 1, pp. 107–116, Jan. 1999.
- [32] M. Li and R. H. Taylor, "Optimum robot control for 3D virtual fixture in constrained ENT surgery," in *Proc. Int. Conf. Med. Image Comput. Comput.-Assisted Intervention*, 2003, pp. 165–172.
- [33] A. Agustinos *et al.*, "Visual servoing of a robotic endoscope holder based on surgical instrument tracking," in *Proc. 5th IEEE RAS/EMBS Int. Conf. Biomed. Robot. Biomechatronics*, 2014, pp. 13–18.
- [34] A. Krupa *et al.*, "Autonomous 3-D positioning of surgical instruments in robotized laparoscopic surgery using visual servoing," *IEEE Trans. Robot. Autom.*, vol. 19, no. 5, pp. 842–853, Oct. 2003.
- [35] P. Li *et al.*, "Development of a robotic endoscope holder for nasal surgery," in *Proc. IEEE Int. Conf. Inf. Autom.*, 2013, pp. 1194–1199.
- [36] J. Chan *et al.*, "Foot-controlled robotic-enabled endoscope holder for endoscopic sinus surgery: A cadaveric feasibility study," *Laryngoscope*, vol. 126, no. 3, pp. 566–569, 2016.
- [37] W. Lin *et al.*, "Modeling, design and control of an endoscope manipulator for FESS," in *Proc. IEEE/RSJ Int. Conf. Intell. Robots Syst.*, 2015, pp. 811–816.